Theoretical Insights into the Reduction of Azurin Metal Site with Unnatural Amino Acid Substitutions

Yang Wei and Pengfei Li*

Department of Chemistry and Biochemistry, Loyola University Chicago, Chicago, Illinois 60660, United States

Abstract

Copper-containing proteins play crucial roles in biological systems. Azurin is a copper-containing protein which has a Type 1 copper site that facilitates electron transfer in the cytochrome chain. Previous research has highlighted the significant impact of mutations in the axial Met121 of the copper site on the reduction potential. However, the mechanism of this regulation has not been fully established. In this study, we employed theoretical modeling to investigate the reduction of the Type 1 copper site, focusing on how unnatural amino acid substitutions at Met121 influence its behavior. Our findings demonstrated a strong linear correlation between electrostatic interactions and the reduction potential of the copper site, which indicates that the perturbation of the reduction potential is primarily influenced by electrostatic interactions between the metal ion and the ligating atom. Furthermore, we found that CF/π and CF…H interactions could induce subtle changes in geometry and hence impact the electronic properties of the systems under study. In addition, our calculations suggest the coordination mode and ion-ligand distance could significantly impact the reduction potential of the copper site. Overall, this study offers valuable insights into the structural and electronic properties of the Type 1 copper site, which could potentially guide the design of future artificial catalysts.

Keywords

Azurin, unnatural amino acids, Type 1 copper site, reduction, electrostatics, theoretical

Highlights

- Linear correlation between electrostatics and the reduction potential of azurin
- Fluorine-involved interactions subtly change the properties of the metal site
- Coordination mode of Cu site would significantly impact its reduction potential

Graphic Abstract

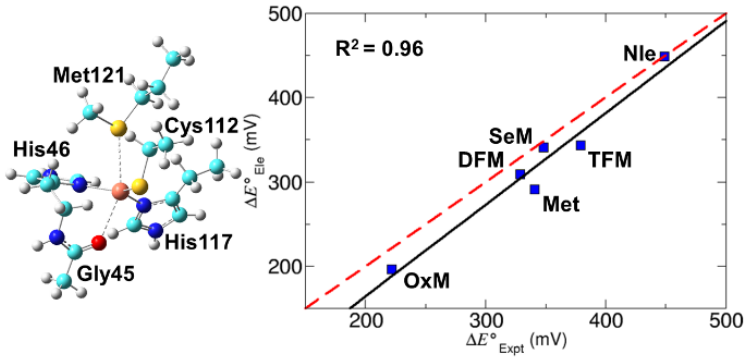

Synopsis for Graphic Abstract The strong correlation observed between the experimental reduction potentials for both azurin and its five mutants, and the reduction energies resulting from electrostatic interactions between the metal ion and ligating atoms, strongly suggests that electrostatic interactions play a dominant role in influencing the reduction potential of T1Cu.

Introduction

Copper-containing proteins play important roles in various biological processes such as electron transfer,[1-5] catalysis,[6, 7] and signaling.[8-10] One of the most common copper sites in proteins is the type 1 copper (T1Cu) center, which is found in a wide range of proteins such as the blue copper proteins (BCPs)[11-15] and multicopper oxidases (MCOs).[16, 17]

Azurin, a small copper-containing protein, is present in *Pseudomonas, Bordetella, and Alcaligenes* bacteria. It facilitates electron transfer between enzymes involved in the cytochrome chain. At its core, Azurin contains a crucial T1Cu center (see **Figure 1**), essential for its functions, making it a prototype for studying electron transfers mediated by T1Cu proteins. In Azurin, the T1Cu coordinates with two histidines (His46 and His117) and one cysteine (Cys112) in the equatorial positions, giving rise to its characteristic blue color.[18, 19] Additionally, it weakly bonds with methionine (Met121) and backbone carbonyl glycine (Gly45) in the axial positions. The stable coordination of these ligands during the switching of oxidation states between Cu^{2+} and Cu^{+} results in a small reorganization energy, facilitating the ET transfer processes.[20-23]

Moreover, the free energy change of the ET reaction can be fine-tuned by adjusting the redox potential of the metal site. Previous studies have involved mutating the axial Met121 in Azurin to its unnatural amino acid isostructural analogs, including oxomethionine (OxM), selenomethionine (SeM), difluoromethionine (DFM), trifluoromethionine (TFM), and norleucine (Nle) (**Figure 1**). These mutations resulted in a considerable variation of ~230 mV in the reduction potential.[24, 25] Importantly, these mutations have had a minimal impact on the protein structure, which allowed researchers to isolate the effect of residue 121 from other parameters like steric and geometric factors and solvent exposure. As a result of these investigations, a strong correlation was discovered between the hydrophobicity of the axial ligand and the reduction potential of the copper site.[25]

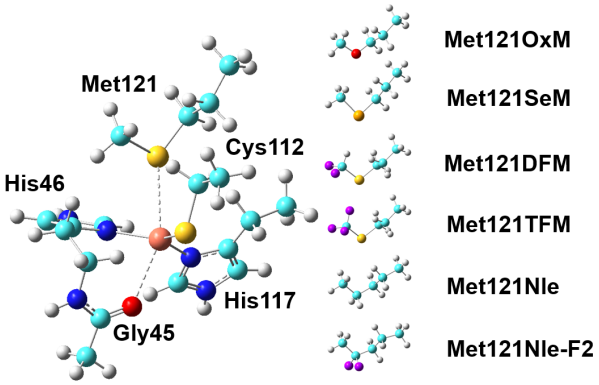

Figure 1. The type 1 copper (T1Cu) site in Azurin (Az). It has Met121 in in the axial position. Its unnatural analogs: oxomethionine (OxM), selenomethionine (SeM), difluoromethionine (DFM), trifluoromethionine (TFM), norleucine (Nle), and Nle-F2, are also shown and investigated in the present study. The metal site structure was built based on PDB entry: 1JZF,[26] with the amino acids were capped by changing the Cα atoms to methyl groups and the geometry of Met121 was optimized afterwards. The axial coordination bonds are shown in dash lines.

Although such a correlation was discovered, the molecular mechanism of such a regulation has not been fully understood. Moreover, previous QM/MM study successfully reproduced the redox potentials of different mutants and suggested these regulations are mainly electrostatic in

nature.[20] In the present study, we conducted a comprehensive investigation of the electrostatic interactions between residue 121 and the Cu complex, using quantum mechanical (QM) and molecular mechanical (MM) calculations. Our results reveal a compelling linear correlation between the electrostatic interaction between the metal ion and ligating atom, and the reduction potential of the T1Cu site. We observed a transition from a combination of electrostatic and vdW interactions between Met121OxM/Met121SeM/Met121DFM/Met121TFM and the Cu site to pure vdW interactions between Met121Nle and the Cu site. Furthermore, our research highlighted intriguing C-F/π and C-F/H interaction pairs in the Met121DFM mutant, which were found to influence both the geometry and electronic properties of the protein. Additionally, we delved into the impact of 5-coordinated and 6-coordinated Cu sites, analyzing how the reduction energy is dependent on the metal-ligand distance. The results indicated that the reduction energy of the 6-coordinated Cu site is more sensitive to perturbations in the ligand environment. Understanding the factors that govern reduction potential holds significant promise for gaining insights into the electronic properties and reactivity of metal sites, thereby guiding relevant molecular designs. Our findings offer valuable molecular insights into the physical properties of the T1Cu site and have potential implications for designing artificial metalloproteins with tailored reactivity.

Methods

PDB entry 1JZF was used to model the T1Cu site of *Pseudomonas aeruginosa* azurin, which is a X-ray structure with a resolution of 1.5 Å.[26] Hydrogen atoms were added by using GaussView. Alongside the wild-type, we investigated five mutants: Met121OxM, Met121SeM, Met121DFM, Met121TFM, Met121Nle (see **Figure 1**). These mutations were shown to induce minimal structural perturbation, as confirmed by experimental measurements including ultraviolet-visible (UV-Vis), electron paramagnetic resonance (EPR), and X-ray absorption spectra (XAS).[27] It is reasonable to presume that residues beyond the first coordination sphere exert a consistent background effect on the reduction potentials of these mutants. Given our focus on discerning differences rather than absolute values of reduction potentials, we specifically examined the first coordination shell of the T1Cu site, encompassing Cu^{2+}, Gly45, His46, His117, Cys112, and Met121 (see **Figure 1**). Accordingly, the mutants were manually generated based on the PDB entry 1JZF. To model the metal site, we used a Cα truncated model, where the Cα atoms were substituted with methyl groups. Because Gly45 coordinates to the Cu^{2+} ion with its backbone carbonyl group, the peptide bond between Gly45 and His46 was kept, while the -NH group of Gly45 and -CO group of His46 were replaced by hydrogen atoms. To mimic the protein environment, during the optimization, the Cα atom of residue 121, Cu^{2+} ion, and other residues were kept frozen, with only the other atoms of the residue 121 were allowed to move.

This approach was adopted because residue 121 exhibits notably weaker interaction with the Cu site compared to other ligating residues. Therefore, mutating residue 121 would have minimal impact on the coordination modes of other metal site residues, as confirmed by experimental data from UV-Vis, EPR, and XAS measurements.[27] Meanwhile, given its weak coordination to the metal site, it was crucial to treat residue 121 as flexible during optimization. The optimization was carried out using the Berny algorithm with GEDIIS.[28] Following the optimization of residue 121 at the Cu^{2+} site, the same optimized geometry was employed to calculate the energy of the metal site in the reduced state (i.e., Cu^{+} state). We believe this treatment is reasonable because of the minimal structural changes caused by the reduction of T1Cu in Azurin.[20, 23, 25] By taking the energy difference between the two states, we obtained the reduction energy for each of the wild-type and mutants.

Density functional theory (DFT) calculations were performed using the Gaussian 16 program (version C.01),[29] employing the ωB97XD functional.[30] The ωB97XD functional could well model the weak interactions between residue 121 and the metal site due to it includes atom-atom dispersion correction. The Cu atom was treated with the def2-TZVP basis set,[31] while all other atoms were treated with the 6-31G* basis set.[32] Our tests demonstrated that extending Def2-TZVP to S atoms minimally affected the Cu-S distance between Cu and Met121, in agreement with a previous study showing insensitivity to the basis set.[33] To account for the protein environment around the metal site, the PCM implicit solvent model[34] with a dielectric constant of 4.0 was utilized.[35] The nature of the stationary points was verified by frequency analyses. The optimized structures and coordinates can be found in the supporting information (SI). In particular, the optimized structures and coordinates of all the systems listed in **Table 1** (below) are included in the SI.

Results and Discussion

Table 1 presents the optimized distances between the Cu ion and ligating atoms in residue 121 (denoted as $R_{Cu\text{-}R121(a)}$) for both the wild-type and the five mutants of Azurin. For the DFM mutation, two cases were studied, with Met121DFM$_d$ and Met121DFM$_u$ represent the DFM residue in the downward and upward configuration, respectively, with more details are provided below. Due to the Met121Nle mutation coordinates to copper ion through the CH_2 group, the distance between copper and the closest atom in the CH_2 group is reported. **Table 1** also indicated that the calculated relative reduction energy (ΔΔE) among the mutants successfully reproduces the experimental trend of reduction potential,[25] thus affirming the reliability of the current approach in modeling the redox property of the T1Cu site. Previous study indicates the reduction potential of the Met121DFM system is sensitive to the environment.[25] Our calculations indicate the Met121DFM$_d$ system showed better agreement with experimentally determined reduction potential than the Met121DFTM$_u$ system as it showed the second lowest reduction potential among the series (**Table 1**), implying it is the dominant structure of the Met121DFM system. In addition, the closely matched values in ΔΔE and $R_{Cu\text{-}R121(a)}$ between Met121 and Met121SeM imply their comparable covalencies, which aligns with the findings from a previous study.[33]

Table 1. Selected Bond Lengths (unit: Å) and Energies (unit: kcal/mol) of the Type 1 Cu Site of Azurine and Mutants

	QM calculations			Exp.[a]		
	$R_{Cu\text{-}R121(a)}$ (Å)	ΔE (kcal/mol)	ΔΔE[b] (kcal/mol)	E° (mV)	ΔG[c] (kcal/mol)	ΔΔG[b] (kcal/mol)
Met121OxM	3.05	-89.58	4.25	222	-5.12	5.23
Met121	3.21	-90.26	3.57	341	-7.86	2.49
Met121SeM	3.28	-90.66	3.17	348	-8.03	2.33
Met121DFM$_d$	3.31	-89.71	4.12	329	-7.59	2.77
Met121DFM$_u$	3.52	-91.46	2.36			
Met121TFM	3.58	-91.61	2.22	379	-8.74	1.61
Met121Nle	2.52[d]	-93.82	0.00	449	-10.35	0.00
Met121Nle-F2	2.61[d]	-89.45	4.37	N/A		

[a] Measured at pH=4, with the data from Ref. [25]; [b] with respect to Met121Nle; [c] Based on the Nernst equation $\Delta G = -nFE^\circ$; [d] Distance to the closest atom in Residue 121.

Among all the studied systems, the optimized Met121OxM exhibits the smallest $R_{Cu\text{-}R121(a)}$ value as 3.05 Å. This result can be attributed to the relatively small van der Waals (VDW) radii and strong electronegativity of O (1.55 Å, 3.50 $\sqrt{eV}$) in comparison to those of S (1.80 Å, 2.44 $\sqrt{eV}$) and Se (1.90 Å, 2.48 $\sqrt{eV}$) atoms.[36, 37] In order to gain insights into the influence of electrostatic interactions on the reduction energy, we performed calculations to determine the electrostatic energy between the metal ion and the ligating atom of residue 121. These calculations were based on their respective electrostatic potential (ESP) charges by considering the excellent performance of ESP charges in modeling intermolecular electrostatic interactions. Specifically, the electrostatic energy was computed using Coulomb's law, which allowed us to examine the electrostatic contributions to the overall reduction energy:

$$E_{Ele} = 332\frac{q_1 q_2}{r}$$

Herein, q_1 represents the charge of Cu, q_2 denotes the charge of the coordinate atom of residue 121, and r refers to $R_{Cu\text{-}R121(a)}$. q_1 and q_2 are given in atomic units, and r is in Å. The conversion factor 332 was used to convert the energy unit to kcal/mol. To prevent unrealistic charges on the metal ion, as it is buried within the metal site, we conducted separate Merz-Kollman population analyses[38, 39] for residue 121 and the remaining complex based on the optimized structures of the complexes. This treatment is reasonable due to the relatively large $R_{Cu\text{-}R121(a)}$ value (> 3 Å, see **Table 1**), suggesting a noncovalent interaction between them.[20, 25, 40, 41] As mentioned earlier, we only optimized residue 121 while keeping the remaining part of the complex frozen. However, the distance between Cu and the ligating atom in Met121 ($R_{Cu\text{-}R121(a)}$) in its reduced state (Cu^+ state) is 4.46 Å after optimization, contrary to the QM/MM study, which reported an RMSD of less than 0.1 Å for the heavy atoms in the active site of the azurin protein after Cu^{2+} reduction.[20] The reason for this discrepancy is that we did not explicitly consider the protein environment in our QM modeling. As a result, for each system we used the optimized structure of the oxidized state for the corresponding reduced state. We believe this treatment is reasonable due to the minimal structural changes caused by the reduction of T1Cu in Azurin.[20, 23, 25]

Using the aforementioned settings, we conducted separate calculations of the electrostatic energy for the ion and ligating atom in both the oxidized and reduced states. By subtracting these energies, we derived the reduction energy values, as summarized in **Table 2**. Remarkably, the computed electrostatic energy relative to Nle (ΔE_{Ele}) demonstrates a highly significant correlation with the experimental reduction potential, yielding a R-squared value of 0.96 and a slope of 1.09 (**Figure 2**). These results strongly suggest that electrostatic interactions between the metal ion and ligating atom play a predominant role in determining the difference in reduction potential.

Table 2. The ESP charges and Reduction Energies Calculated Based on the ESP Charges

	$Q(Cu^{2+})$ (e)	$Q(Cu^{+})$ (e)	$Q_{R121(a)}$[a] (e)	ΔE_{Ele}[b] (kcal/mol)	E°_{Ele}[c] (mV)
without Res121	0.248	0.119	N/A	0.00	439
Met121OxM	0.248	0.119	-0.399	5.61	196
Met121	0.248	0.119	-0.256	3.42	291
Met121SeM	0.248	0.119	-0.174	2.28	341
$MET121DFM_d$	0.248	0.119	-0.232	3.01	309
$MET121DFM_u$	0.248	0.119	-0.251	3.05	307
MET121TFM	0.248	0.119	-0.187	2.23	343
Met121Nle	0.248	0.119	0.013[d]	-0.22	449
Met121Nle-F2	0.248	0.119	-0.244[d]	4.00	266

[a] the charge of the coordination atom of residue121; [b] based on Coulomb's law; [c] The reduction potentials due to electrostatic interactions, the values were calculated by treating the experimental reduction potential of Nle as reference and shifting the other values respect to Nle; [d] the charge of the closest atom to metal ion.

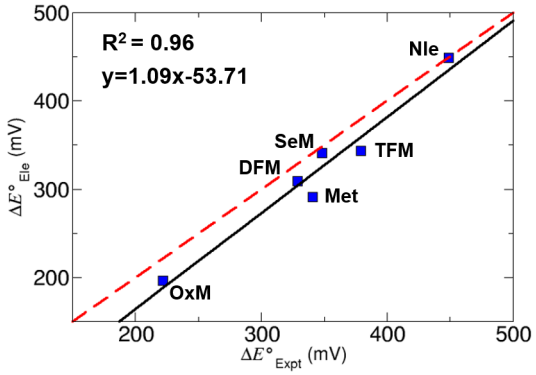

Figure 2. The experimental reduction potential *versus* the reduction energy due to electrostatic interaction between the metal ion and ligating atom for azurin and the five mutants. For the case of Met121DFM, the Met121DFM$_d$ configuration was used. To facilitate comparison, all the values were obtained by treating the Met121Nle system as the reference.

As indicated in **Table 2**, the S atom in Met121 possesses a charge of -0.256 e. In contrast, the presence of the -CF_3 group in Met121TFM diminishes the nucleophilicity of its coordinating S atom, which bears an ESP charge of -0.187 e. This alteration weakens the electrostatic interaction between the metal center and Met121TFM. Furthermore, the CF/π interaction between the CF_3 group and His46 in the Met121TFM mutant elongates the F… π distance, as depicted in **Figure 3B**. This observation is consistent with a DFT study of interactions between fluorinated alkane and benzene, which revealed a 0.7 Å longer C-F/π distance compared to the C-H/π distance in the optimized structures.[42] Consequently, the presence of the CF_3 group pushes the Met121TFM group away from Cu^{2+}, leading to a longer $R_{Cu\text{-}R121(a)}$ distance of 3.58 Å when compared to the wild-type system ($R_{Cu\text{-}R121(a)}$ = 3.21 Å, as shown in **Table 1**). This spatial change, together with the less negative charge on the ligating atom, results in a significantly reduced electrostatic interaction between the metal ion and Met121TFM than between the metal ion and Met121.

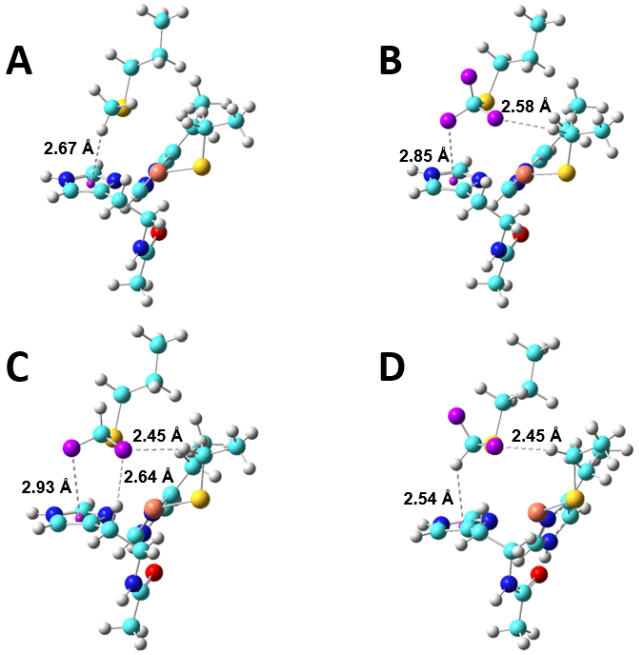

Figure 3. The optimized structures of the (A) Met121, (B)MET121TFM, (C) MET121DFM$_d$ where the two -F groups point downwards, and (D) MET121DFM$_u$ where the two -F groups point upwards. Selected C-F/π distances and C-F/H distances are shown in black numbers.

Previous study indicated the reduction potential of DFM is sensitive to the environment.[25] Besides the Met121TFM system, the CF/π interaction was also observed in the Met121DFM$_d$ system when the two -F groups were oriented towards histidine, as depicted in **Figure 3C**. An analysis of the different conformations of Met121DFM (DFM$_d$ and DFM$_u$) revealed that its $R_{Cu\text{-}R121(a)}$ distance is sensitive to the environment. Specifically, the Met121DFM$_d$ system contains two $R_{CH\ldots F}$ interaction pairs, resulting in a shorter $R_{Cu\text{-}R121(a)}$ value of 3.31 Å compared to MET121DFM$_u$ (3.52 Å), which only contains one $R_{CH\ldots F}$ interaction pair (**Figure 3** and **Table 1**). This observation indicates that this distance is sensitive to the environment. In addition, all these $R_{CH\ldots F}$ distances are smaller than the sum of VDW radii of F (1.47 Å) and H (1.20 Å),[43] suggesting the occurrence of CF…H interactions. Previous studies have shown that the interaction energy of CF…H is stronger than that of CH…H or CF…F.[44] These results underscore the subtle roles of different interactions in influencing the geometry and hence the reduction potential of the metal site.

Furthermore, acknowledging fluorine's higher electronegativity compared to oxygen, we expanded our investigation to include the Met121Nle-F2 mutant (see **Figure 1**). Encouragingly, our QM calculations predicted that this mutant exhibits an even lower redox potential than Met121OxM (**Table 1**). However, such a trend could not be solely attributed to electrostatic interactions, as suggested in **Table 2**. These findings suggest the involvement of additional subtle factors or interactions beyond electrostatics in influencing the redox potential of the Met121Nle-F2 mutant. These insights may be helpful for relevant experimental studies in the future.

A previous study demonstrated a direct correlation between the reduction potential of the T1Cu site in Azurin and the logP value of residue 121 in octanol-water systems.[25] The logP, defined based on the partition coefficient (P), is delineated below:

$$\log P = \log_{10} \frac{[\text{solute}]_{\text{octanol}}}{[\text{solute}]_{\text{water}}} \quad (1)$$

When the solute is evenly dispersed between octanol and water, P equals 1, resulting in a logP value of zero. Hydrophobic residues typically yield logP values greater than 0, indicating increased hydrophobicity. Conversely, hydrophilic residues exhibit logP values less than 0. Furthermore, P is directly related to the transfer free energy of the solute between octanol and water:

$$[\text{solute}]_{\text{water}} \xrightarrow{\Delta G_{\text{T}}} [\text{solute}]_{\text{octanol}} \quad (2)$$

When ΔG_{T} is zero, the solute achieves equal distribution between octanol and water, resulting in a P value of 1. Notably, P equates to the equilibrium constant K.

$$P = K = \frac{[\text{solute}]_{\text{octanol}}}{[\text{solute}]_{\text{water}}} = e^{-\frac{\Delta G_{\text{T}}}{RT}} \quad (3)$$

$$\log P = \log_{10} K = \log_{10} e^{-\frac{\Delta G_{\text{T}}}{RT}} \quad (4)$$

$$\Delta G_{\text{T}} = -RT \ln P \quad (5)$$

We showed the logP values for different residues in **Table 3**, along with their corresponding ΔG_{T} values. Remarkably, there exists a strong correlation between ΔG_{T} (X axis) and ΔG (Y axis), as illustrated in **Figure 4**. It's reasonable to expect that a residue with a ligating atom carrying a larger negative charge would exhibit greater hydrophilicity. Additionally, it would stabilize Cu^{2+} more effectively than Cu^{+}, resulting in a less negative reduction energy (defined as $E(Cu^{+})$-$E(Cu^{2+})$) and reduction free energy (ΔG). Simultaneously, the residue would have a smaller equilibrium constant (K), as $K = \frac{[\text{solute}]_{\text{octanol}}}{[\text{solute}]_{\text{water}}}$, leading to a decrease in the logP value. Given that $\Delta G_{\text{T}} = -RT \ln P$, where there is a negative sign, an increase in ΔG_{T} would occur. Therefore, a notable correlation between ΔG and ΔG_{T} is observed in **Figure 4**.

Table 3. The logP and ΔG_{T} values for wild-type T1Cu and mutants.

	Exp. E° (mV)	ΔG[a] (kcal/mol)	logP[b]	ΔG_{T}[c] (kcal/mol)
Met121OxM	222	-5.12	0.481	-0.66
Met121	341	-7.86	1.371	-1.88
Met121SeM	348	-8.03	1.571	-2.16
Met121DFM	329	-7.59	1.817	-2.49
Met121TFM	379	-8.74	2.48	-3.40
Met121Nle	449	-10.35	2.81	-3.86

[a]Based on the Nernst equation $\Delta G = -nFE^{\circ}$
[b]From Ref[25]
[c]Based on equation 5 at T = 300 K.

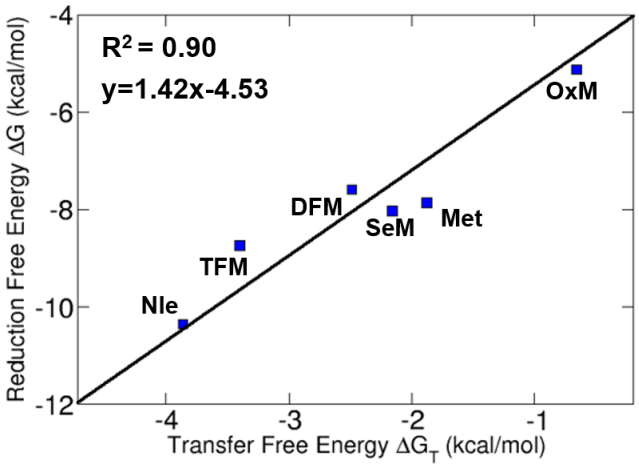

Figure 4. Correlation between ΔG and ΔG_T values for the wild-type T1Cu and mutants. The fitted line is shown as solid line, while its equation and R^2 value are shown on the left-up corner.

Although an excellent R^2 was observed between ΔG and ΔG_T, the slope deviates from 1.0, with ΔG exhibiting a larger range compared to ΔG_T. This discrepancy may arise from the intrinsic differences in the nature of these two free energies. Typically, the solvation of a molecule involves both enthalpy change (ΔH) and entropy change (ΔS), with the hydrophobic effect primarily driven by ΔS. Consequently, ΔG_T encompasses a significant contribution from both ΔH and ΔS with enthalpy-entropy compensation.[45-49] In contrast, the reduction potential of Cu^{2+} in Azurin is primarily influenced by ΔH, with minimal contribution from ΔS due to the limited reorganization of the metal site during reduction. This disparity leads to a slope deviating from 1.0 in the correlation between ΔG and ΔG_T, with ΔG having a larger range than ΔG_T. This difference may be attributed to the enthalpy-entropy compensation effect in ΔG_T, where ΔS counteracts ΔH, resulting in a smaller overall free energy change compared to ΔG.

Cu^{2+} typically exhibits a coordination number of five or six. To explore the impact of coordination mode and ion-ligand distance on the reduction energy of Cu^{2+}, we conducted calculations on two illustrative systems: $[Cu(H_2O)_5]^{2+}$ and $[Cu(H_2O)_6]^{2+}$ (see **Figure 5**), representing five- and six-coordinated copper sites, respectively. We anticipate that insights gleaned from these systems might be applicable to biological Cu sites with both five and six coordinated ligands. Both systems were thoroughly optimized, and their optimized structures and coordinates are provided in the SI. Afterwards, for each system, we performed a rigid scan along the Cu^{2+}-water distance to assess the reduction energy changes. The presence of the Jahn-Teller effect necessitated separate consideration of the ligands in the equatorial position (XY-plane) and axial position (Z-axis), as they exert different influences on the reduction energy of the copper ion. Consequently, we carried out two scans for each system, one with a water molecule at the equatorial position and the other with a water molecule at the axial position. By using the reduction energy at the equilibrium geometry as a reference, we computed the relative reduction energy during the scanning of the Cu^{2+}-water distance. The results of these calculations are presented in **Figure 5**.

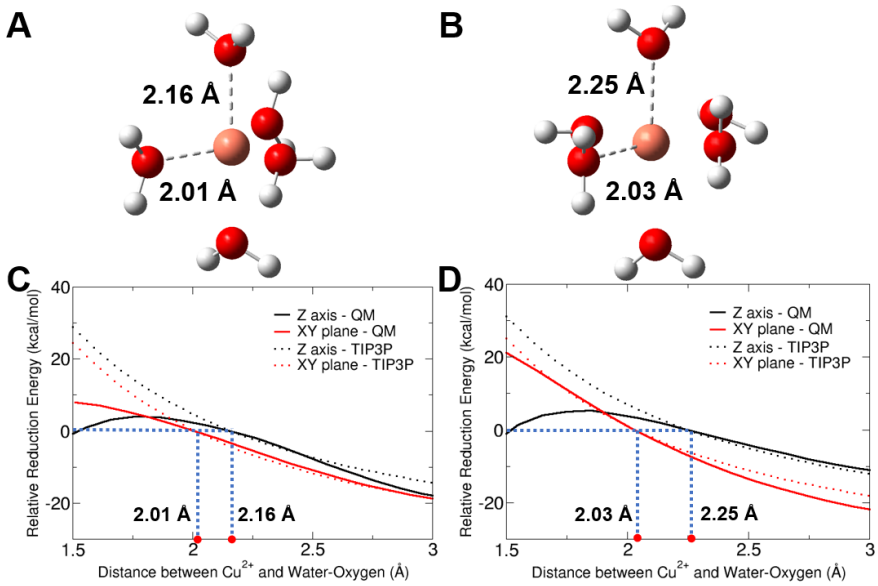

Figure 5. The optimized geometries of the (A) $[Cu(H_2O)_5]^{2+}$ and (B) $[Cu(H_2O)_6]^{2+}$ systems. The distance between copper and water in the equatorial or axial position is denoted in black number. Additionally, the relative reduction energy (kcal/mol) is presented, defined as the energy difference between the reduced state and oxidized state, i.e. $E(Cu^+)$-$E(Cu^{2+})$, with respect to the equilibrium position, along with the rigid scan of $R_{Cu\text{-}ligand}$ in the (C) $[Cu(H_2O)_5]^{2+}$ and (D) $[Cu(H_2O)_6]^{2+}$ systems. In this context, a positive value indicates that the system stabilizes Cu^{2+} more than Cu^+ compared to the equilibrium state. Conversely, a negative value suggests the opposite scenario, where the system stabilizes Cu^+ over Cu^{2+} relative to the equilibrium position. In panels C and D, the black and red solid curves are the relative reduction energies obtained by QM calculations. The black and red dash curves are the relative reduction energies calculated by using classical force fields. The blue dash lines are marks for the equilibrium distances.

Indeed, our findings indicate that the water molecule in the equatorial position exerts a significantly different influence on the reduction energy of the metal center compared to the water in the axial position. Specifically, for both the $[Cu(H_2O)_5]^{2+}$ and $[Cu(H_2O)_6]^{2+}$ systems, the curve representing the axial ligands exhibits a maximum. This suggests that there exists an optimal distance for the axial ligands to maximize their reduction energy. This observed maximum cannot be solely explained by electrostatic interactions, as electrostatic interactions would predict a monotonous increase in the curve as the ion-ligand distance decreases, without a maximum point. On the other hand, the curve for the equatorial ligands does not exhibit a maximum within the plotted range. Instead, it shows a monotonous increase as the ion-ligand distance decreases. These results highlight the nuanced interplay of various factors beyond electrostatic interactions in determining the reduction energy with respect to ion-ligand distances.

Furthermore, we observed significant differences between the $[Cu(H_2O)_5]^{2+}$ and $[Cu(H_2O)_6]^{2+}$ systems. Specifically, in the $[Cu(H_2O)_5]^{2+}$ system, the curve of the equatorial ligand displayed a comparable slope to that of the axial ligand at the corresponding equilibrium distance. This suggests that the equatorial and axial ligands exert similar influences on the reduction energy of the metal site. This finding aligns with a recent study investigating how mutations on the equatorial His117 impact the reduction potential of the T1Cu site in Azurin.[23] The study observed that the

His117Ntr mutation caused a ~200 meV shift in reduction potential at pH=7 and ~100 meV shift at pH=4. These magnitudes are comparable to the influence of the mutation on the axial Met121 residue (see **Table 1**). In contrast, for the $[Cu(H_2O)_6]^{2+}$ system, the equatorial ligand exhibited a significantly larger slope compared to the axial ligand at the corresponding equilibrium distance. This suggests that the number of equatorial ligands has a strong impact on the electrochemical properties of the copper center. The reduction energy of the 6-coordinated Cu^{2+} is more sensitive to the ligand environment than that of the 5-coordinated Cu^{2+} for the Cu^{2+}-aqueous complexes.

The properties of azurins are largely impacted by the primary coordination sphere and secondary coordination sphere.[22, 27, 50, 51] Our results implied that one can tune the redox potentials and hence chemical reactivity of a Cu-site by engineering its coordination modes and ion-ligand distances. This agrees with a previous study by Lu et al.[50] Specifically, it was found that the mutation of H46E and M121H transforms the coordination mode of wild type azurin from trigonal planar geometry to a tetragonally distorted square planar geometry, leading to its reactivity in S-nitrosylation which was not observed in the wild type azurin. This study highlighted that we the strategy for regulating the reactivity and reduction potential of the Cu site by tuning its coordination mode. Similarly, our results suggest that engineering the T1Cu site into a 6-coordinated octahedral metal site could result in a different reduction potential and consequently alter its chemical reactivity.

To further elucidate the influence of electrostatic interactions on the reduction potentials of $[Cu(H_2O)_5]^{2+}$ and $[Cu(H_2O)_6]^{2+}$, we conducted calculations of the relative reduction energy along the scans using classical force fields. In this approach, the Cu^{2+} and Cu^{+} ions were assumed to have the same VDW parameters. The TIP3P water model[52] was utilized to represent the water molecules, with fixed geometry and atomic charges. Specifically, the three atoms in the moving water were assumed to lie in the same plane as the copper ion, with the central axis of the water molecule crossing the copper ion. The results are presented in panels C and D of **Figure 5** as red and black dashed curves. In these calculations, we considered only the influence of electrostatic interactions on the reduction potential. Comparing the results of the QM calculations with classical force fields, we observed a reasonably good agreement in the long-range (i.e. the solid curve agrees well with the dash curve beyond the equilibrium distance). However, as the distance approached the short-range, the agreement started to deviate. This trend is consistent with the notion that in the long-range, the point-charge approximation can reasonably model molecular interactions, but it fails in the short-range. Consequently, based on the point-charge representation, one can estimate the influence of the ligand on the reduction potential, as demonstrated in **Table 2**.

Furthermore, we utilized the QM method to calculate the reduction energy for the T1Cu site along with the metal ion and ligand distance, employing OxM, Met, and Nle as examples. The results demonstrated distinct trends for the Met121OxM, Met121, and Met121Nle systems (**Figure 6**). Notably, Met121OxM and Met121 exhibited similar trends, indicating a decline in energy with ion-ligand distance increases. In contrast, Met121Nle showed an almost unchanged reduction energy along with ion-ligand distance, revealing the absence of electrostatic interactions in Met121Nle. As a result, the reduction potential remained unaffected by changes in the ion-ligand distance. Both Met121OxM and Met121 exhibited slopes, with the former showing a larger slope. This difference can be attributed to the stronger electrostatic attraction between Cu and oxygen in Met121OxM, when compared to the electrostatic attraction between Cu and sulfur in

Met121. These findings emphasize the significant role of electrostatic interactions in influencing the relationship between the reduction potential of the T1Cu site and the ion-ligand distance.

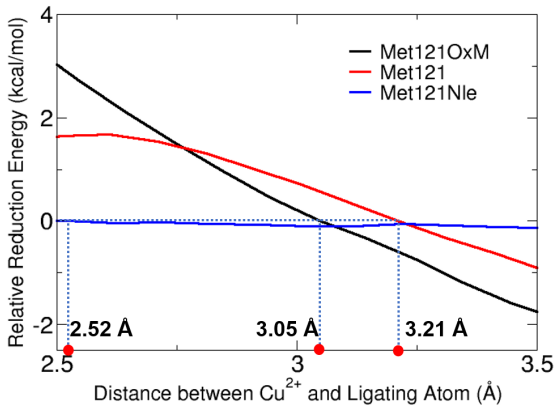

Figure 6. The relative reduction energy (kcal/mol) along the rigid scan of $R_{Cu\text{-}ligand}$ in the T1Cu center of Azurin. The reduction energy is defined as $E(Cu^{+}) - E(Cu^{2+})$, with the relative reduction energy is respect to the equilibrium position during the rigid scan. A positive value indicates that the system stabilizes Cu^{2+} more than Cu^{+} when compared to the equilibrium state. On the other hand, a negative value indicates the opposite scenario, where the system favors Cu^{+} over Cu^{2+} relative to the equilibrium position. The blue dash lines are marks for the equilibrium distances of the three systems.

Conclusions

In this study, we conducted a systematic investigation of the redox properties of T1Cu through theoretical calculations. By modeling the wild-type *Pseudomonas aeruginosa* azurin and its five mutants, we successfully reproduced the trend in experimentally measured reduction potentials of the metal site. Our findings revealed that the major difference introduced by mutations is caused by electrostatic interactions between the metal ion and ligating atoms. Among these mutations, the interaction between copper ion and Met121Nle is governed by van der Waals interactions. Moreover, our results indicated the CF/π and CF…H interactions in Met121DFM and Met121TFM mutants could perturb the equilibrium geometry and consequently regulate the reduction potential of the metal site. Our results also indicated that the coordination mode and ion-ligand distances can significantly impact the reduction potential of the metal site. Our study underscores the nuanced roles that various interactions play in determining the intricate physical properties of the metal site. These insights would offer valuable guidance for future engineering endeavors focused on copper sites.

Acknowledgement

We acknowledge Loyola for providing the start-up funds (to P.L.). We are grateful for the computational resources offered by the XSEDE platform, which was supported by the National Science Foundation under grant number ACI-1548562. Specifically, this study made use of the CPU resources on Expanse at the San Diego Supercomputer Center under allocation numbers TG-BIO210105. Additionally, we acknowledge the assistance of ChatGPT (https://openai.com/blog/chatgpt) in optimizing the language of the manuscript.

Funding
This research was supported by the Loyola start-up funds (to P.L.).

References

1. Beinert, H., Copper A of Cytochrome c Oxidase, A Novel, Long-Embattled, Biological Electron-Transfer Site. *Eur. J. Biochem.* **1997,** *245*, 521-532.
2. Houser, R. P.; Young, V. G.; Tolman, W. B., A thiolate-bridged, fully delocalized mixed-valence dicopper (I, II) complex that models the CuA biological electron-transfer site. *J. Am. Chem. Soc.* **1996,** *118*, 2101-2102.
3. Farver, O.; Pecht, I., Long-range intramolecular electron transfer in azurins. *Proc. Natl. Acad. Sci.* **1989,** *86*, 6968-6972.
4. Monari, A.; Very, T.; Rivail, J.-L.; Assfeld, X., Effects of mutations on the absorption spectra of copper proteins: a QM/MM study. *Marco Antonio Chaer Nascimento: A Festschrift from Theoretical Chemistry Accounts* **2014**, 39-47.
5. Mitra, S.; Ainavarapu, S. R. K.; Dasgupta, J., Long-Range Charge Delocalization Mediates the Ultrafast Ligand-to-Metal Charge Transfer Dynamics at the Cu2+-Active Site in Azurin. *J. Phys. Chem. B* **2022,** *126*, 5390-5399.
6. Wang, F.; Zhang, Y.; Liu, Z.; Du, Z.; Zhang, L.; Ren, J.; Qu, X., A biocompatible heterogeneous MOF–Cu catalyst for in vivo drug synthesis in targeted subcellular organelles. *Angew. Chem. Int. Ed.* **2019,** *58*, 6987-6992.
7. Gawande, M. B.; Goswami, A.; Felpin, F.-X.; Asefa, T.; Huang, X.; Silva, R.; Zou, X.; Zboril, R.; Varma, R. S., Cu and Cu-based nanoparticles: synthesis and applications in catalysis. *Chem. Rev.* **2016,** *116*, 3722-3811.
8. Ackerman, C. M.; Chang, C. J., Copper signaling in the brain and beyond. *J. Biol. Chem.* **2018,** *293*, 4628-4635.
9. Gaier, E. D.; Eipper, B. A.; Mains, R. E., Copper signaling in the mammalian nervous system: synaptic effects. *J. Neurosci. Res.* **2013,** *91*, 2-19.
10. Kardos, J.; Héja, L.; Simon, Á.; Jablonkai, I.; Kovács, R.; Jemnitz, K., Copper signalling: causes and consequences. *Cell Commun. Signal.* **2018,** *16*, 1-22.
11. Solomon, E. I.; Hadt, R. G., Recent advances in understanding blue copper proteins. *Coord. Chem. Rev.* **2011,** *255*, 774-789.
12. Solomon, E. I.; Szilagyi, R. K.; DeBeer George, S.; Basumallick, L., Electronic Structures of Metal Sites in Proteins and Models: Contributions to Function in Blue Copper Proteins. *Chem. Rev.* **2004,** *104*, 419-458.
13. Marshall, N. M.; Garner, D. K.; Wilson, T. D.; Gao, Y.-G.; Robinson, H.; Nilges, M. J.; Lu, Y., Rationally tuning the reduction potential of a single cupredoxin beyond the natural range. *Nature* **2009,** *462*, 113-116.
14. Hosseinzadeh, P.; Tian, S.; Marshall, N. M.; Hemp, J.; Mullen, T.; Nilges, M. J.; Gao, Y.-G.; Robinson, H.; Stahl, D. A.; Gennis, R. B., A purple cupredoxin from Nitrosopumilus maritimus containing a mononuclear type 1 copper center with an open binding site. *J. Am. Chem. Soc.* **2016,** *138*, 6324-6327.
15. Arciero, D. M.; Pierce, B. S.; Hendrich, M. P.; Hooper, A. B., Nitrosocyanin, a red cupredoxin-like protein from Nitrosomonas europaea. *Biochem.* **2002,** *41*, 1703-1709.
16. Sakurai, T.; Kataoka, K., Basic and applied features of multicopper oxidases, CueO, bilirubin oxidase, and laccase. *Chem. Rec.* **2007,** *7*, 220-229.
17. Quintanar, L.; Stoj, C.; Taylor, A. B.; Hart, P. J.; Kosman, D. J.; Solomon, E. I., Shall we dance? How a multicopper oxidase chooses its electron transfer partner. *Acc. Chem. Res.* **2007,** *40*, 445-452.
18. Shadle, S. E.; Penner-Hahn, J. E.; Schugar, H. J.; Hedman, B.; Hodgson, K. O.; Solomon, E. I., X-ray absorption spectroscopic studies of the blue copper site: metal and ligand K-edge studies to probe the origin of the EPR hyperfine splitting in plastocyanin. *J. Am. Chem. Soc.* **1993,** *115*, 767-776.
19. Ryde, U.; Olsson, M. H.; Roos, B. O.; Borin, A. C., A theoretical study of the copper–cysteine bond in blue copper proteins. *Theor. Chem. Acc.* **2001,** *105*, 452-462.

20. Shen, L.; Zeng, X.; Hu, H.; Hu, X.; Yang, W., Accurate quantum mechanical/molecular mechanical calculations of reduction potentials in azurin variants. *J. Chem. Theory Comput.* **2018,** *14*, 4948-4957.
21. Hong, G.; Ivnitski, D. M.; Johnson, G. R.; Atanassov, P.; Pachter, R., Design parameters for tuning the type 1 Cu multicopper oxidase redox potential: insight from a combination of first principles and empirical molecular dynamics simulations. *J. Am. Chem. Soc.* **2011,** *133*, 4802-4809.
22. Liu, J.; Chakraborty, S.; Hosseinzadeh, P.; Yu, Y.; Tian, S.; Petrik, I.; Bhagi, A.; Lu, Y., Metalloproteins Containing Cytochrome, Iron–Sulfur, or Copper Redox Centers. *Chem. Rev.* **2014,** *114*, 4366-4469.
23. Yu, Y.; Marshall, N. M.; Garner, D. K.; Nilges, M. J.; Lu, Y., Tuning reduction potentials of type 1 copper center in azurin by replacing a histidine ligand with its isostructural analogues. *J. Inorg. Biochem.* **2022,** *234*, 111863.
24. Berry, S. M.; Ralle, M.; Low, D. W.; Blackburn, N. J.; Lu, Y., Probing the role of axial methionine in the blue copper center of azurin with unnatural amino acids. *J. Am. Chem. Soc.* **2003,** *125*, 8760-8768.
25. Garner, D. K.; Vaughan, M. D.; Hwang, H. J.; Savelieff, M. G.; Berry, S. M.; Honek, J. F.; Lu, Y., Reduction potential tuning of the blue copper center in Pseudomonas aeruginosa azurin by the axial methionine as probed by unnatural amino acids. *J. Am. Chem. Soc.* **2006,** *128*, 15608-15617.
26. Crane, B. R.; Di Bilio, A. J.; Winkler, J. R.; Gray, H. B., Electron Tunneling in Single Crystals of Pseudomonas aeruginosa Azurins. *J. Am. Chem. Soc.* **2001,** *123*, 11623-11631.
27. Mirts, E. N.; Bhagi-Damodaran, A.; Lu, Y., Understanding and Modulating Metalloenzymes with Unnatural Amino Acids, Non-Native Metal Ions, and Non-Native Metallocofactors. *Acc. Chem. Res.* **2019,** *52*, 935-944.
28. Li, X.; Frisch, M. J., Energy-represented direct inversion in the iterative subspace within a hybrid geometry optimization method. *J. Chem. Theory Comput.* **2006,** *2*, 835-839.
29. Frisch, M. J.; Trucks, G. W.; Schlegel, H. B.; Scuseria, G. E.; Robb, M. A.; Cheeseman, J. R.; Scalmani, G.; Barone, V.; Petersson, G. A.; Nakatsuji, H.; Li, X.; Caricato, M.; Marenich, A. V.; Bloino, J.; Janesko, B. G.; Gomperts, R.; Mennucci, B.; Hratchian, H. P.; Ortiz, J. V.; Izmaylov, A. F.; Sonnenberg, J. L.; Williams; Ding, F.; Lipparini, F.; Egidi, F.; Goings, J.; Peng, B.; Petrone, A.; Henderson, T.; Ranasinghe, D.; Zakrzewski, V. G.; Gao, J.; Rega, N.; Zheng, G.; Liang, W.; Hada, M.; Ehara, M.; Toyota, K.; Fukuda, R.; Hasegawa, J.; Ishida, M.; Nakajima, T.; Honda, Y.; Kitao, O.; Nakai, H.; Vreven, T.; Throssell, K.; Montgomery Jr., J. A.; Peralta, J. E.; Ogliaro, F.; Bearpark, M. J.; Heyd, J. J.; Brothers, E. N.; Kudin, K. N.; Staroverov, V. N.; Keith, T. A.; Kobayashi, R.; Normand, J.; Raghavachari, K.; Rendell, A. P.; Burant, J. C.; Iyengar, S. S.; Tomasi, J.; Cossi, M.; Millam, J. M.; Klene, M.; Adamo, C.; Cammi, R.; Ochterski, J. W.; Martin, R. L.; Morokuma, K.; Farkas, O.; Foresman, J. B.; Fox, D. J. *Gaussian 16 Rev. C.01*, Wallingford, CT, 2016.
30. Chai, J.-D.; Head-Gordon, M., Long-range corrected hybrid density functionals with damped atom-atom dispersion corrections. *Phys. Chem. Chem. Phys.* **2008,** *10*, 6615-6620.
31. Weigend, F.; Ahlrichs, R., Balanced basis sets of split valence, triple zeta valence and quadruple zeta valence quality for H to Rn: Design and assessment of accuracy. *Phys. Chem. Chem. Phys.* **2005,** *7*, 3297-3305.
32. Rassolov, V. A.; Ratner, M. A.; Pople, J. A.; Redfern, P. C.; Curtiss, L. A., 6-31G* basis set for third-row atoms. *J. Comput. Chem.* **2001,** *22*, 976-984.
33. Sarangi, R.; Gorelsky, S. I.; Basumallick, L.; Hwang, H. J.; Pratt, R. C.; Stack, T. D. P.; Lu, Y.; Hodgson, K. O.; Hedman, B.; Solomon, E. I., Spectroscopic and Density Functional Theory Studies of the Blue−Copper Site in M121SeM and C112SeC Azurin: Cu−Se Versus Cu−S Bonding. *J. Am. Chem. Soc.* **2008,** *130*, 3866-3877.
34. Mennucci, B.; Tomasi, J., Continuum solvation models: A new approach to the problem of solute's charge distribution and cavity boundaries. *J. Chem. Phys.* **1997,** *106*, 5151-5158.
35. Torres, R. A.; Lovell, T.; Noodleman, L.; Case, D. A., Density Functional and Reduction Potential Calculations of Fe4S4 Clusters. *J. Am. Chem. Soc.* **2003,** *125*, 1923-1936.
36. Batsanov, S. S., Van der Waals radii of elements. *Inorg. Mater.* **2001,** *37*, 871-885.

37. Little Jr, E. J.; Jones, M. M., A complete table of electronegativities. *J. Chem. Educ.* **1960,** *37*, 231.
38. Singh, U. C.; Kollman, P. A., An approach to computing electrostatic charges for molecules. *J. Comput. Chem.* **1984,** *5*, 129-145.
39. Besler, B. H.; Merz Jr., K. M.; Kollman, P. A., Atomic charges derived from semiempirical methods. *J. Comput. Chem.* **1990,** *11*, 431-439.
40. Solomon, E. I.; Randall, D. W.; Glaser, T., Electronic structures of active sites in electron transfer metalloproteins: contributions to reactivity. *Coord. Chem. Rev.* **2000,** *200*, 595-632.
41. Warren, J. J.; Lancaster, K. M.; Richards, J. H.; Gray, H. B., Inner-and outer-sphere metal coordination in blue copper proteins. *J. Inorg. Biochem.* **2012,** *115*, 119-126.
42. Kawahara, S.-i.; Tsuzuki, S.; Uchimaru, T., Theoretical Study of the C−F/π Interaction: Attractive Interaction between Fluorinated Alkane and an Electron-Deficient π-System. *J. Phys. Chem. A* **2004,** *108*, 6744-6749.
43. Bondi, A. v., van der Waals volumes and radii. *J. Phys. Chem.* **1964,** *68*, 441-451.
44. Tsuzuki, S.; Uchimaru, T.; Mikami, M.; Urata, S., Ab Initio Calculations of Intermolecular Interaction of CHF3 Dimer: Origin of Attraction and Magnitude of CH/F Interaction. *J. Phys. Chem. A* **2003,** *107*, 7962-7968.
45. Gallicchio, E.; Kubo, M. M.; Levy, R. M., Entropy-enthalpy compensation in solvation and ligand binding revisited. *changes* **1998,** *5*, 13-15.
46. Exner, O., Entropy–enthalpy compensation and anticompensation: solvation and ligand binding. *Chem. Commun.* **2000**, 1655-1656.
47. Chodera, J. D.; Mobley, D. L., Entropy-enthalpy compensation: role and ramifications in biomolecular ligand recognition and design. *Annu. Rev. Biophys.* **2013,** *42*, 121-142.
48. Ryde, U., A fundamental view of enthalpy–entropy compensation. *MedChemComm* **2014,** *5*, 1324-1336.
49. Peccati, F.; Jiménez-Osés, G., Enthalpy–entropy compensation in biomolecular recognition: A computational perspective. *ACS omega* **2021,** *6*, 11122-11130.
50. Tian, S.; Liu, J.; Cowley, R. E.; Hosseinzadeh, P.; Marshall, N. M.; Yu, Y.; Robinson, H.; Nilges, M. J.; Blackburn, N. J.; Solomon, E. I.; Lu, Y., Reversible S-nitrosylation in an engineered azurin. *Nat. Chem.* **2016,** *8*, 670-677.
51. Van Stappen, C.; Dai, H.; Jose, A.; Tian, S.; Solomon, E. I.; Lu, Y., Primary and Secondary Coordination Sphere Effects on the Structure and Function of S-Nitrosylating Azurin. *J. Am. Chem. Soc.* **2023,** *145*, 20610-20623.
52. Neria, E.; Fischer, S.; Karplus, M., Simulation of activation free energies in molecular systems. *J. Chem. Phys.* **1996,** *105*, 1902-1921.